Supporting Information

Unraveling the Role of Lithium in Enhancing the Hydrogen Evolution Activity of MoS_2: Intercalation vs. Adsorption

Longfei Wu,[†] Nelson Y. Dzade,[‡§] Miao Yu,[†] Brahim Mezari,[†] Arno J. F. van Hoof,[†] Heiner Friedrich,[⊥] Nora H. de Leeuw,[‡§] Emiel J. M. Hensen,[†] and Jan P. Hofmann[†*]

[†]Laboratory for Inorganic Materials and Catalysis, Department of Chemical Engineering and Chemistry, Eindhoven University of Technology, P.O. Box 513, 5600 MB Eindhoven, The Netherlands

[‡]Faculty of Geosciences, Utrecht University, Princetonlaan 8A, 3584 CB Utrecht, The Netherlands

[§]School of Chemistry, Cardiff University, Main Building, Park Place, CF10 3AT, Cardiff, United Kingdom

[⊥]Laboratory of Materials and Interface Chemistry, Department of Chemical Engineering and Chemistry, Eindhoven University of Technology, P.O. Box 513, 5600 MB, Eindhoven, The Netherlands

*Email address of corresponding author: J.P.Hofmann@tue.nl

TABLE OF CONTENTS

Part I: Experimental and computational details

Chemicals

Ammonium heptamolybdate tetrahydrate ($(NH_4)_6Mo_7O_{24} \cdot 4H_2O$, > 99.3 %) and $LiNO_3$ (≥ 98.0 %) were purchase from Merck. Activated carbon (NORIT RX-3 extra) was sieved to 125 – 250 µm and had a pore size of 1 $cm^3\ g^{-1}$. γ-alumina was sieved to 75-125 µm and had a pore size of 0.65 $cm^3\ g^{-1}$. Sulfuric acid (H_2SO_4, 99.999 %) was purchased from Sigma-Aldrich. To prepare a 0.1M H_2SO_4 electrolyte, 2.665 mL sulfuric acid was added to a certain amount of Milli-Q water (18 MΩ cm) and filled up to 500 mL in a volumetric flask. All chemicals and materials were used as received without further purification.

Catalyst preparation

The Li_xMoS_2 catalysts were prepared by impregnation of activated carbon (pore volume 1 $cm^3\ g^{-1}$) with aqueous solutions of the precursors. Typically, a certain amount of $(NH_4)_6Mo_7O_{24} \cdot 4H_2O$ and $LiNO_3$ were dissolved in 3 mL water, and the as-prepared solution was transferred and filled up to 10 mL in a volumetric flask. 500 µL precursor solution was impregnated to 500 mg activated carbon. Then, the catalysts were left on the roller band for 2 h and dried overnight at 110 °C. The dried catalysts (100 mg) were sulfurized in 10 % H_2S in H_2 (40 ml min^{-1}) at 350 °C under atmospheric pressure for 2 h with a heating rate of 6 °C min^{-1}. Li/Mo composition was determined by ICP-OES analysis as shown in Tables S1 and 2.

Figure S1. Scheme of the synthetic process of Li_xMoS_2 on carbon support.

Materials characterization

XPS measurements were conducted on a ThermoScientific K-Alpha spectrometer with a monochromatic X-ray source (E(Al Kα) = 1486.6 eV). The spectra were calibrated by setting the sp^3 C 1s peak of adventitious carbon to 284.6 eV and fitted by CasaXPS software using a Shirley background subtraction and Gaussian (70%)-Lorentzian (30%) line shapes. Survey scans were collected at constant pass energy of 200 eV and region scans at 50 eV. ^{7}Li NMR experiments were performed on a Bruker Avance DMX500 instrument operating at 194 MHz for ^{7}Li in a magnetic field of 11.7 Tesla. The measurements were carried out using a 2.5-mm MAS probe head with a sample rotation rate of 20 kHz. ^{7}Li 1D spectra were recorded with a single pulse sequence with a 90° pulse duration of 5 µs and an interscan delay of 320 s. Higher interscan delays showed no significant increase in intensity. 2D exchange

(NOESY) spectra were recorded by use of a pulse sequence $p1$-d_0-$p1$-t_{mix}-$p1$-acquisition (90° pulse $p1$ = 5 µs, delay time d_0 = 2.5 µs and mixing times t_{mix} of 10 µs, 100 µs, 100 ms, and 1s). An interscan delay of 3 s was chosen. The ^{7}Li chemical shift is referred to a saturated aqueous LiCl solution. The different samples were loaded in a 2.5-mm zirconia NMR rotor in a glovebox and closed with an SP1 cap. Afterwards, the rotor was transported to the NMR probe head under N_2 atmosphere. TEM images were acquired with a Tecnai 20 transmission electron microscope (FEI company, now Thermo Fisher Scientific) equipped with a LaB_6 filament and operated at an acceleration voltage of 200 kV. The sulfurized catalysts were transported to an argon filled glovebox and dispersed in dry n-hexane, then a few droplets were placed on Cu TEM grids. The grid was transported in a GATAN vacuum transfer holder (Model number CHVT3007). Infrared spectra were recorded on a Nicolet FT-IR spectrometer equipped with a liquid N_2-cooled MCT detector. IR pellets (D = 13 mm) were prepared from catalysts impregnated on γ-alumina (pore volume 0.65 cm^3 g^{-1}) support, the samples were pressed as a self-supporting wafers of around 10 mg cm^{-2}. Then, the pellets were placed in a home-made *in-situ* cell equipped with CaF_2 windows, and sulfurized at 350 °C for 2 h (6 °C min^{-1}) with 10 % H_2S in H_2 (40 mL min^{-1}). After cooling down to room temperature, the cell was flushed with N_2 for 15 mins. Afterwards, the sample was heated again to 350 °C for 1 h (6 °C min^{-1}), and the cell as evacuated overnight to reach a pressure below 10^{-5} mbar. The MCT detector was cooled down with liquid N_2, and molecular NO was passed through a liquid N_2/1-propanol cold trap and introduced via a calibrated sample loop connected to a pressure gauge. Spectra were recorded (256 scans, resolution: 2 cm^{-1}) after each aliquot up to an equilibrium of around 0.6 mol (NO) mol (Mo)$^{-1}$. All spectra were baseline corrected in the range of 1200-2200 cm^{-1} in OMNIC software and presented in absorbance mode.

X-ray absorption spectroscopy (XAS) was performed at the Dutch-Belgian beamline BM26A (DUBBLE) at the European Synchrotron ESRF, operating at 6 GeV with a beam current of 200 mA. Li_xMoS_2/C samples were mounted as self-supporting wafers by dispersing 50 mg catalysts in 50 mg cellulose. Then, the mixtures were grinded and pressed by a manual press and sealed with Kapton foil in a glovebox. Mo foil was used as a reference for energy calibration, all spectra were collected in transmission mode at the Mo K-edge (20 keV). EXAFS spectra were background subtracted with Athena and fitted with Artemis software[30]. Scattering paths were calculated by FEFF6[30] from molybdenite (MoS_2) crystal structure from American Mineralogist Crystal Structure Database[31]. The fitting range of Mo K-edge was Δk = 2-12 Å^{-1} and ΔR = 1-3 Å. Plotted spectra were not phase-corrected and have a k-weight of 3. 1T' to 2H phase ratio was determined by the coordination number (CN) ratio of Mo-Mo (distorted) and Mo-Mo bond.

Electrochemical measurements

Electrochemical tests were performed in a three-electrode electrochemical cell with a saturated $Hg(I)/Hg_2Cl_2(s)/KCl$ electrode as reference, Pt foil as counter electrode and catalysts modified glassy carbon electrodes (GCE) as working electrodes (electrode preparation details can be found in SI, Part IV). The reference electrode was calibrated with respect to a reversible hydrogen electrode (RHE), and has a potential of +0.269 V vs. RHE. HER measurements were carried out in Ar saturated 0.1 M H_2SO_4, CV and LSV curves were recorded at scan rate of 50 and 5 mV s^{-1}, respectively. Electrochemical impedance spectroscopy (EIS) was carried out from 100 kHz to 1 Hz at open circuit potential (OCP) (Figure S15). To evaluate the electrochemical active surface area (ECSA), CV curves were recorded from V_{OCP} −0.05 to V_{OCP} +0.05 V with scan rates of 20, 40, 60, 80, 100 mV s^{-1}. The double layer capacitance (C_{dl}) was extracted by plotting $\Delta j = j_a - j_c$ (j_a and j_c corresponds to anodic and cathodic current densities, respectively) at V_{OCP} against the CV scan rates with the following equation: $\frac{j_a - j_c}{2} = C_{dl}\frac{dE}{dt}$. The current density for both CV and LSV curves was normalized by the geometric surface area of the electrode. For HER stability tests, a total weight of 5 mg Li_xMoS_2/C catalyst was mixed with 40 μL 20 % wt. Nafion® solution to yield a slurry, which subsequently was daubed uniformly on carbon fiber paper (CFP) and dried in vacuum at 100 ˚C for 24h. Afterwards, the CFP electrode was attached on copper wire by conductive silver paste and sealed with nonconductive epoxy for HER measurements.

TOF calculation

To evaluate the hydrogen evolution reaction (HER) rate per active site and per time (defined as TOF, s^{-1}), the number of active sites (N_{active}) were determined. Here, we assumed that Mo-edges are active sites for HER. Then, based on NO titration curves (Figure S11), we can calculate the fraction of Mo-edges (~0.2 ± 0.02).[1] As the Mo loading amount was determined by ICP-OES, the number of Mo-edges on GCE can be determined by the following equation: $N_{active} = \frac{m \times 0.001 \times wt\% \times N_A}{M\,(Mo)} \times 0.2$, where m is the loading of catalyst on the electrode (0.1 mg in our case), S is the geometric electrode area (0.2826 cm^2 in our case), $wt\ \%$ is the weight percentage of Mo determined by ICP, N_A is the Avogadro constant ($6.022 \times 10^{23}\ mol^{-1}$). The TOF was then determined by the equation $TOF\ (s^{-1}) = \frac{j\ (A\ cm^{-2}) \times S\ (cm^2) \times \frac{1}{2}}{N_{active} \times q_e}$, j was derived from the current generated during HER, S is the geometric surface area of the working electrode, and q_e is the electron charge (1.602×10^{-19} C).

Computational details

First-principles calculations were performed using the Vienna ab-initio simulation (VASP) package,[2,3] a periodic

plane wave DFT code which includes the interactions between the core and valence electrons using via the Projector Augmented Wave (PAW) method.[4] The electronic exchange-correlation potential was calculated using the GGA-PBE functional.[5] Wave functions were expanded in a plane wave basis with a high energy cutoff of 600 eV and the convergence criterion was set to 10^{-6} eV between two ionic steps for the self-consistency process. A vacuum region of 20 Å was added along the normal direction to the MoS_2 monolayers to avoid interactions between adjacent images. The Brillouin zone was sampled using a 9 × 9 × 1 Monkhorst-Pack *k*-point mesh. Van der Waals dispersion forces were accounted for in all calculations through the Grimme DFT-D3 functional,[6] which adds a semi-empirical dispersion potential to the conventional Kohn–Sham DFT energy.[7] In order to obtain the equilibrium lattice constant, full relaxations were conducted on the 2H and 1T MoS_2 monolayers in Figure S18. The lattice constant of the 2H-MoS_2 is 3.168 Å, the bond length of Mo–S and Mo-Mo is 2.415 Å and 3.168 Å, respectively, whereas the lattice constant of the 1T-MoS_2 monolayer is 3.192 Å, where Mo–S and Mo-Mo bond lengths are 2.421 Å and 3.192 Å, respectively. The 2H-MoS_2 is shown to be a semiconductor with a bandgap of 1.59 eV (Figure S18a), whereas the 1T-MoS_2 monolayer is metallic (Figure S18b) in excellent agreement with earlier theoretical predictions.[8] Both valence and conduction bands of the 2H-MoS_2 are composed mainly of the Mo 3d states and some S 3p states, similar to the electronic states around the Fermi level of the 1T-MoS_2. The optimized monolayers were used to truncate the MoS_2 structures to obtain Mo-terminated edges along the $(10\bar{1}0)$-2H and (0001)-1T crystallographic planes for the Gibbs free energy of hydrogen adsorption (ΔG_H) calculations. A vacuum region of 20 Å was added along the normal direction to the Mo-edges to avoid interactions between adjacent images. A single Mo-edge row separated by 15 Å vacuum was considered in the y-direction, so that this layer was also isolated in this direction. The modeled structures involve the monolayer 1T-MoS_2 with increasing lithium ions adsorbed on both sides of the layer, as shown in Figure S18. The surface formation energy ($E_{\text{surf-form}}$) of the Mo-edge surfaces without and with adsorbed Li is calculated using equations (1) and (2) respectively:

$$E_{surf-form} = \frac{E^{relaxed}_{Mo-edge} - nE^{relaxed}_{bulk}}{2A} \quad (1)$$

$$E_{surf-form} = \frac{E^{relaxed}_{Mo-edge\ +\ mLi} - nE^{relaxed}_{bulk} - mE_{Li}}{2A} \quad (2)$$

where $E^{relaxed}_{Mo-edge}$ is the energy of the relaxed slab, $nE^{relaxed}_{bulk}$ is the energy of an equal number (n) of bulk MoS_2 units, mE_{Li} is the energy of an equal number (m) of bulk Li metal (per atom) and A is the area of the surface.

Bader population analyses were carried out using the code developed by Henkelman and co-workers[9] in order to quantify charge changes in the S and Mo atoms after Li adsorption. Insight into the electron density redistributions within the Li_xMoS_2 monolayers due to the adsorption of Li atoms was gained through a differential charge-density difference ($\Delta\rho$) isosurface analysis obtained using equation (3):

$$\Delta\rho = \rho_{Li-MoS_2} - (\rho_{MoS_2} + \rho_{Li-layer}) \quad (3)$$

where ρ is the electronic charge density and the subscripts *Li-MoS_2*, *MoS_2*, and *Li-layer* refer to the adsorbate-substrate Li-MoS_2 monolayer, isolated MoS_2 monolayer and isolated adsorbate Li-layer, respectively. The atomic positions of the isolated MoS_2 monolayer and of the Li array are kept the same as those of the total Li-MoS_2 system, which ensures that the presentation highlights local electron density rearrangement due the adsorption process. Similarly, the insight into local charge rearrangement within the Li_xMoS_2+H system was gained from the electron

density difference isosurfaces (Figure S21) was obtained by subtracting from the electron density of the total Li_xMoS_2+H system, both the electron density of the naked Li_xMoS_2 surface and that of an isolated H atom: $\Delta\rho = \rho(Li_xMoS_2 + H) - [\rho(Li_xMoS_2) + \rho(H)$.

The core-level binding energy (E_{CL}), which is the energy required to remove a core electron from the atom of interest was calculated as the energy difference between two separate calculations (so-called ΔSCF approach)[10, 11] based on the equation: $E_{CL} = E(n_c - 1) - E(n_c)$. The first involves a standard DFT calculation, wherein the number of core electrons corresponds to the unexcited ground state [$E(n_c)$], whereas in the second calculation, one electron is removed from the core of one particular atom and added to the valence or conduction band [$E(n_c - 1)$]. Core-level binding energy shifts (E_{CLS}) represent the changes in binding of specific core electrons (E_{CL}) of atoms of interest compared to reference atoms, which are typically located in a different environment, as per the equation $E_{CLS} = E_{CL} - E_{CL}^{ref}$. The calculated E_{CLS} can be compared directly to X-ray photoelectron spectroscopy (XPS) binding energy shifts in order to gain detailed atomic-level understanding of adsorption sites and structures. However, due to lack of accounting for relativistic effects and screening by the core electrons in the PAW potential (*i.e.* the other core electrons are kept frozen in the configuration for which the PAW potential was generated after a single core electron is excited from the core to the valence) the approach does not yield absolute values for the core level binding energies. But test for variety of systems suggest that calculated core level binding energy shifts (differences in the binding energies) can be estimated well within the XPS experimental accuracy of 0.1 eV using Hartree–Fock (HF) of Density Functional Theory (DFT) based calculations.[12, 13]

The hydrogen evolution reaction (HER) is a classic example of a two-electron transfer reaction with one catalytic intermediate, H* (where * denotes a site on the surface able to bind to hydrogen), and may occur through either the Volmer-Heyrovsky ($H^+ + e^- + H^* \rightarrow H_2 + *$) or the Volmer-Tafel ($2H^* \rightarrow H_2 + 2*$) mechanism.[14] The free energy of $H^+ + e^-$ is the same as that of ½ H_2 at standard conditions.[15, 16] The Gibbs free energy of hydrogen adsorption (ΔG_H), the best known descriptor for the hydrogen evolution activity, was calculated by the free energy with respect to molecular hydrogen including zero-point energy and entropy terms via:

$$\Delta G_H = \Delta E_H + \Delta E_{ZPE} - T\Delta S_H \quad (4)$$

where ΔE_H is the adsorption energy of hydrogen which is defined as:

$$\Delta E_H = E_{MoS_2+H} - E_{MoS_2} - \frac{1}{2}E_{H_2} \quad (5)$$

The vibrational and configurational entropies of the adsorbed H*-intermediate are assumed to be negligible, and thus the entropy difference is simply $\Delta S_H \approx -\frac{1}{2}S_{H_2} = -0.7$ meV K^{-1}, where S_{H_2} is the entropy of molecule hydrogen in gas phase. The zero-point energy of a studied system is defined as the sum over all ground state vibrational modes using the equation:

$$E_{ZPE} = \frac{hc}{2}\sum_{i}^{modes} v_i \quad (6)$$

where h is the Planck constant and ν_i's are the calculated vibrational frequencies. The ground state vibrational frequency of the gas phase H_2 is obtained at 4400 cm^{-1}.[7] Using the calculated vibrational frequencies of H adsorbed on the Li_xMoS_2 (**Table S9**) the ZPE-contribution to the Gibbs free energy of hydrogen adsorption can be calculated

as $\Delta E_{ZPE} = E_{ZPE}^{H} - {}^{1}/_{2}E_{ZPE}^{H_2}$, which we found to be in the range of approximately 0.02−0.06 eV. Evaluating the entropic term at a temperature of 298 K gives $-T\Delta S_H \approx 0.2$ eV, and therefore the correction to the Gibbs free energy of hydrogen adsorption is determined to be approximately in the range of 0.22−0.26 eV on the Li_xMoS_2 systems, which is consistent with previous theoretical predictions.[15, 16]

Part II: ICP-OES analysis

MoS_2 loaded on carbon support: 25 mg sample was weighed and put into a beaker, then 5 mL sulfuric acid (1:1 volume ratio with water) were added. The beaker was placed on a hot plate in the fume cupboard, heated and stirred until the catalyst is dissolved. Afterwards, the solution was cooled down to room temperature, then a few mL of distilled water were added and mixed together. Thereafter, the solution was transferred to a 50 mL volumetric flask and filled up with distilled water. After the carbon residue has settled to the bottom of the flask, the clear solution on top was taken out and diluted 5 times. Table S1 summarizes the ICP-OES analysis results of catalysts loaded on carbon support.

Table S1. ICP-OES analysis results of MoS_2 loaded on carbon support.

Sample name	Mo wt. %	Li wt. %	Li : Mo (molar ratio)
MoS_2/C	8.36	-	-
$Li_{0.14}MoS_2$/C	8.65	0.08	0.14
$Li_{0.29}MoS_2$/C	8.45	0.18	0.29
$Li_{0.48}MoS_2$/C	8.15	0.28	0.48
$Li_{1.00}MoS_2$/C	8.00	0.58	1.00
$Li_{2.06}MoS_2$/C	6.58	0.98	2.06

MoS_2 loaded on alumina support: 25 mg sample was weighed and put into a beaker, then after adding 5 mL sulfuric acid (1:1 volume ratio with water), the beaker was placed on the hot plate in the fume cupboard, heated and stirred until the catalyst was dissolved. The solution was cooled down to room temperature, then a few mL of distilled water were added and mixed together. Afterwards, the solution was transferred to a 50 mL volumetric flask and filled up with distilled water. The as-prepared solution was diluted 5 times for the ICP-OES measurement. Table S2 summarizes the ICP-OES results of catalysts loaded on alumina support.

Table S2. ICP-OES analysis results of MoS_2 loaded on alumina support.

Sample name	Mo wt. %	Li wt. %	Li : Mo (molar ratio)
MoS_2/Al_2O_3	8.28	-	-
$Li_{0.08}MoS_2/Al_2O_3$	8.66	0.66	0.08
$Li_{0.30}MoS_2/Al_2O_3$	8.36	0.18	0.30
$Li_{0.61}MoS_2/Al_2O_3$	8.51	0.38	0.61
$Li_{1.22}MoS_2/Al_2O_3$	7.92	0.70	1.22
$Li_{2.37}MoS_2/Al_2O_3$	7.58	1.30	2.37

Part III: Characterization of Li_xMoS_2 particles

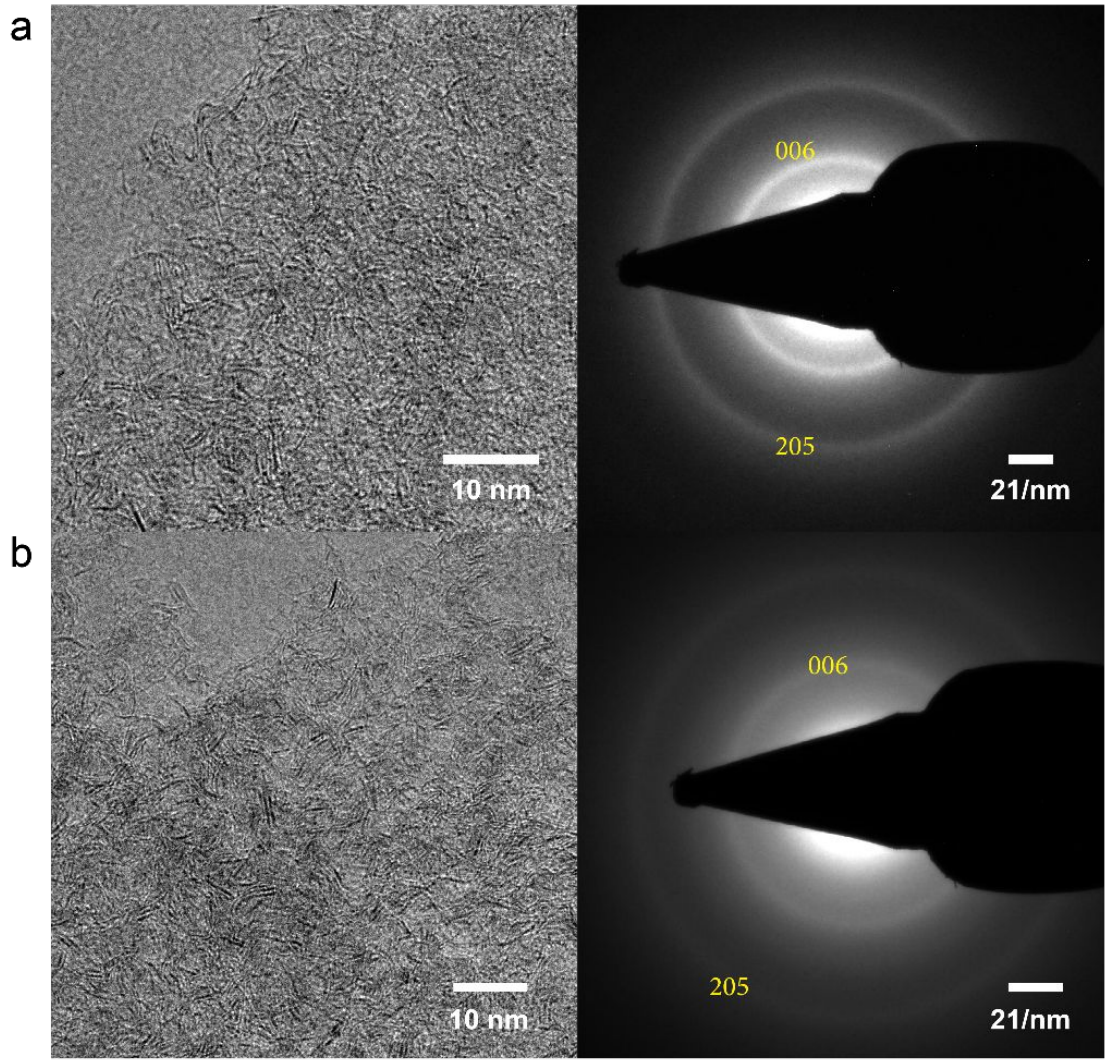

Figure S2. HR-TEM images and corresponding selected area electron diffraction (SAED) patterns of MoS_2 (a) and $Li_{0.29}MoS_2$ (b) on carbon support.

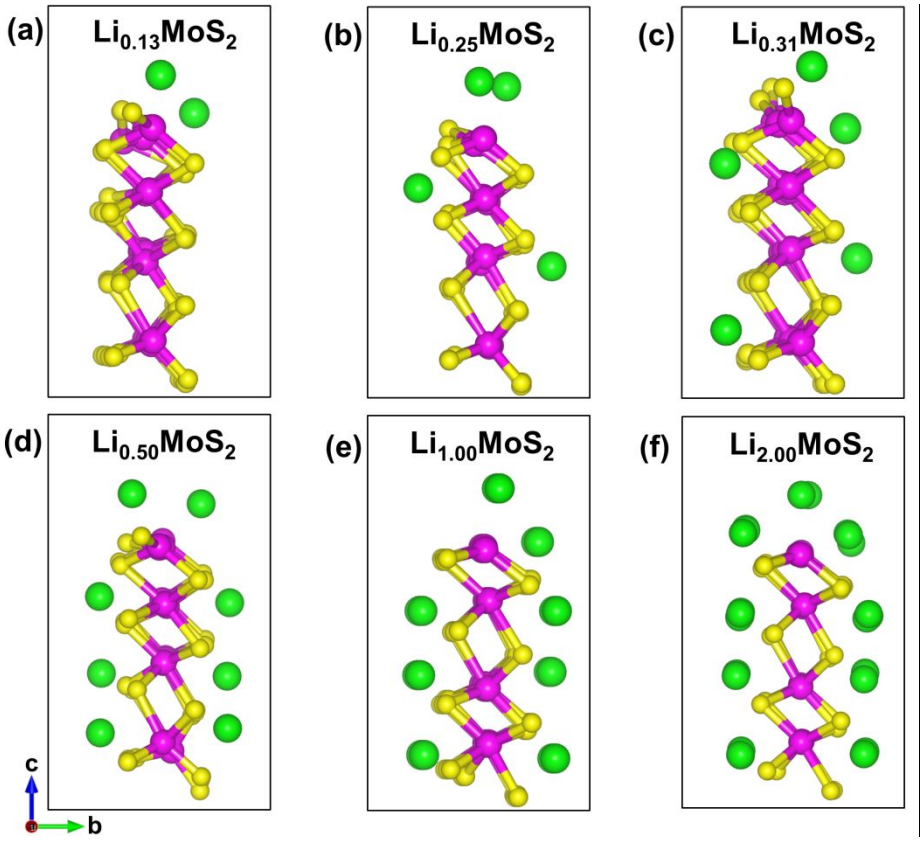

Figure S3. Side view of the optimized structures of Li_xMoS_2 monolayers with increasing Li concentration. a, $Li_{0.13}MoS_2$; b, $Li_{0.25}MoS_2$; c, $Li_{0.31}MoS_2$; d, $Li_{0.50}MoS_2$; e, $Li_{1.00}MoS_2$; f, $Li_{2.00}MoS_2$. A vacuum size of 20 Å was added in the c direction perpendicular to the Mo-edge.

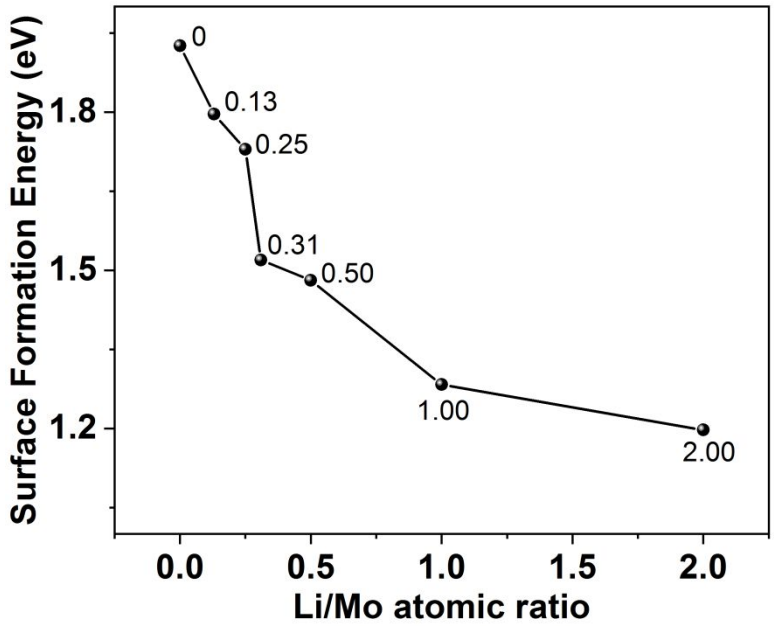

Figure S4. The surface formation energies of Li_xMoS_2 monolayers with increasing Li concentration.

Part IV: Core-level binding energies of Mo 3d and S 2p in Li_xMoS_2

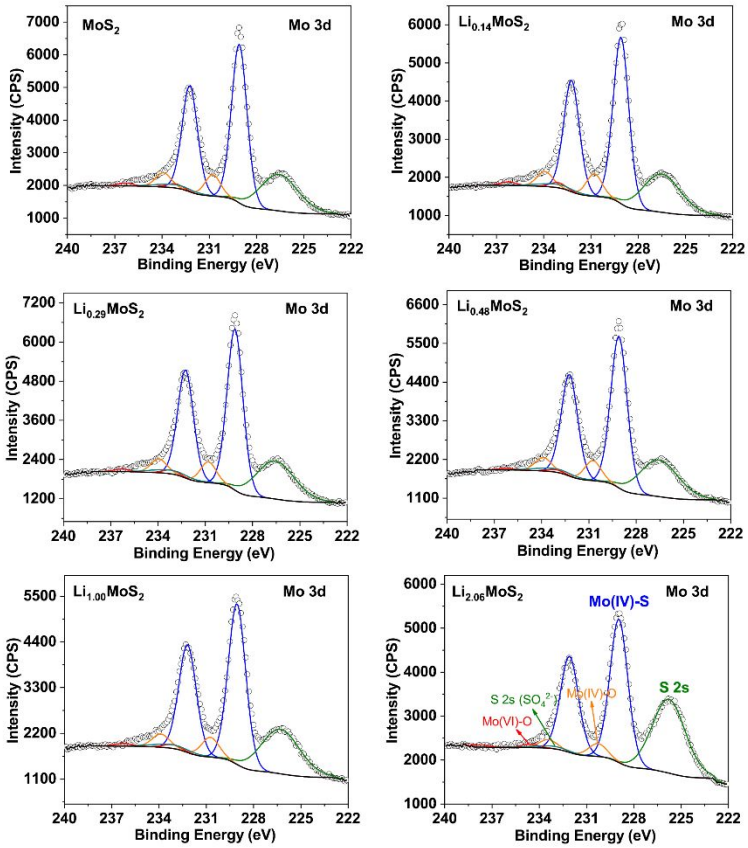

Figure S5. Mo 3d XP spectra for samples with various Li loading on carbon support.

Table S3. Summary for the binding energy of Mo (IV)-S bond with different Li loading on carbon support.

Sample name	Mo (IV)-S Binding Energy (eV)
MoS_2	229.1
$Li_{0.14}MoS_2$	229.1
$Li_{0.29}MoS_2$	229.1
$Li_{0.48}MoS_2$	229.1
$Li_{1.00}MoS_2$	229.0
$Li_{2.06}MoS_2$	228.9

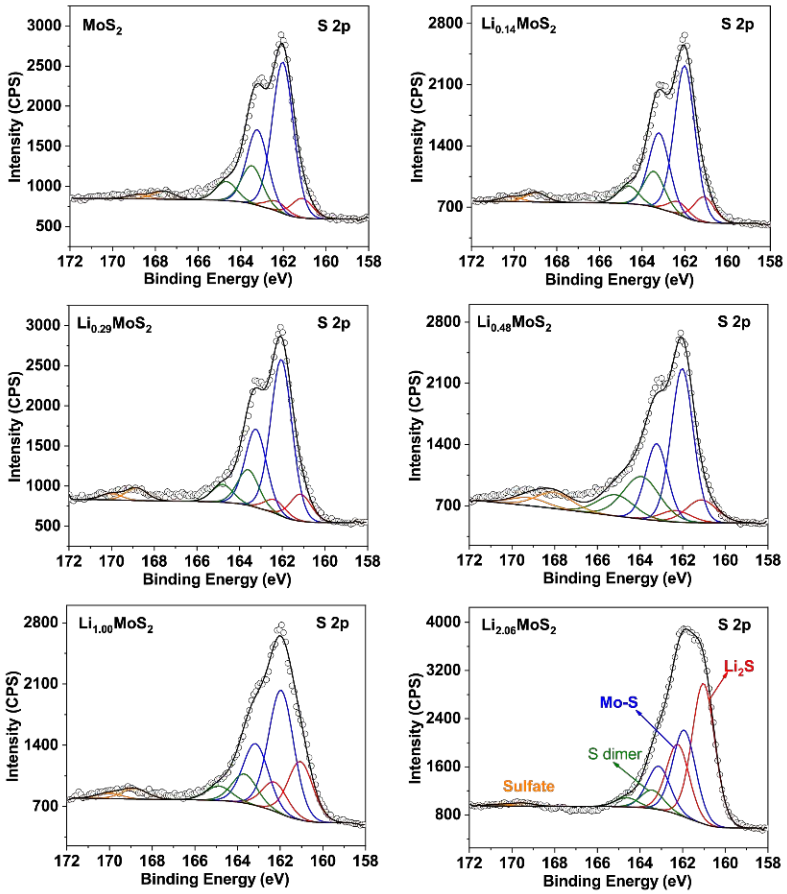

Figure S6. S 2p XP spectra for samples with various Li loading on carbon support.

Table S4. Summary for the atomic percentage of sulfur species based on S 2p spectra.

Sample	% At. Conc. (Electron rich S^{2-})	% At. Conc. (S^{2-})	% At. Conc. (S in S_2^{2-})	% At. Conc. (Sulfate)
MoS_2	9.8	52.8	28.3	9.1
$Li_{0.14}MoS_2$	11.9	53.5	25.7	8.9
$Li_{0.29}MoS_2$	13.2	53.5	23.9	9.5
$Li_{0.48}MoS_2$	11.2	54.6	24.8	9.4
$Li_{1.00}MoS_2$	32.9	37.7	21.2	8.2
$Li_{2.06}MoS_2$	41.3	42.8	12.6	3.3

Table S5: Summary for the DFT-based core-level binding energies (E_{CL}) of Mo-3d and S-2p in Li_xMoS_2 and their shift relative to MoS_2 at different Li concentrations.

Sample name	Mo-3d (eV)	Mo-3d Shift (eV)	S-2p (eV)	S-2p Shift (eV)
MoS_2	222.35	0.00	154.21	0.00
$Li_{0.13}MoS_2$	221.83	−0.52	153.77	−0.44
$Li_{0.25}MoS_2$	221.62	−0.73	153.57	−0.64
$Li_{0.31}MoS_2$	221.54	−0.81	153.47	−0.74
$Li_{0.50}MoS_2$	221.23	−1.12	153.25	−0.96
$Li_{1.00}MoS_2$	220.15	−2.19	152.46	−1.75
$Li_{2.00}MoS_2$	220.08	−2.27	152.54	−1.67

Part V: ^{7}Li MAS NMR

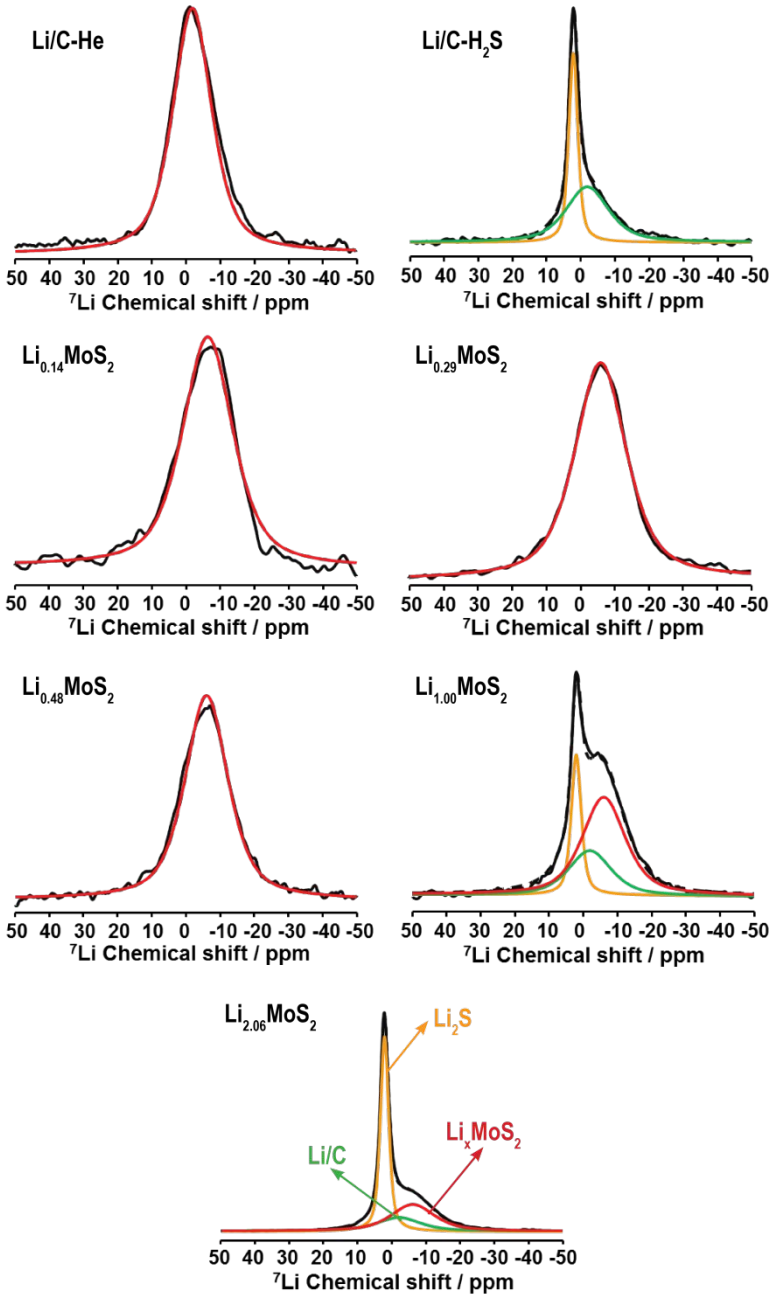

Figure S7. Solid-state Magic Angle Spinning ^{7}Li NMR spectra of Li_xMoS_2 on carbon support. Deconvolution of the NMR peaks are based on Gaussian (40 %)-Lorentz (60 %) line shape functions.

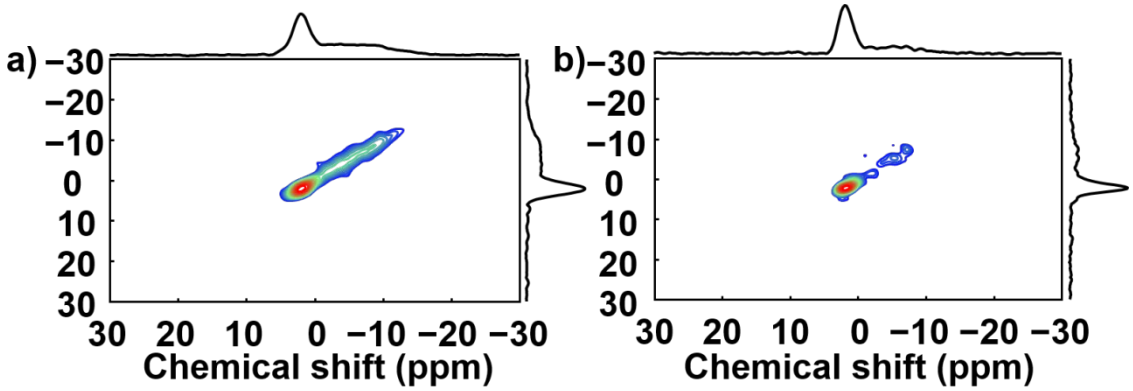

Figure S8. ^{7}Li-^{7}Li MAS 2D exchange (NOESY) NMR spectra of $Li_{2.06}MoS_2$/C with relaxation times of 10 μs (a) and 100 ms (b).

Part VI: FTIR-NO adsorption spectroscopy

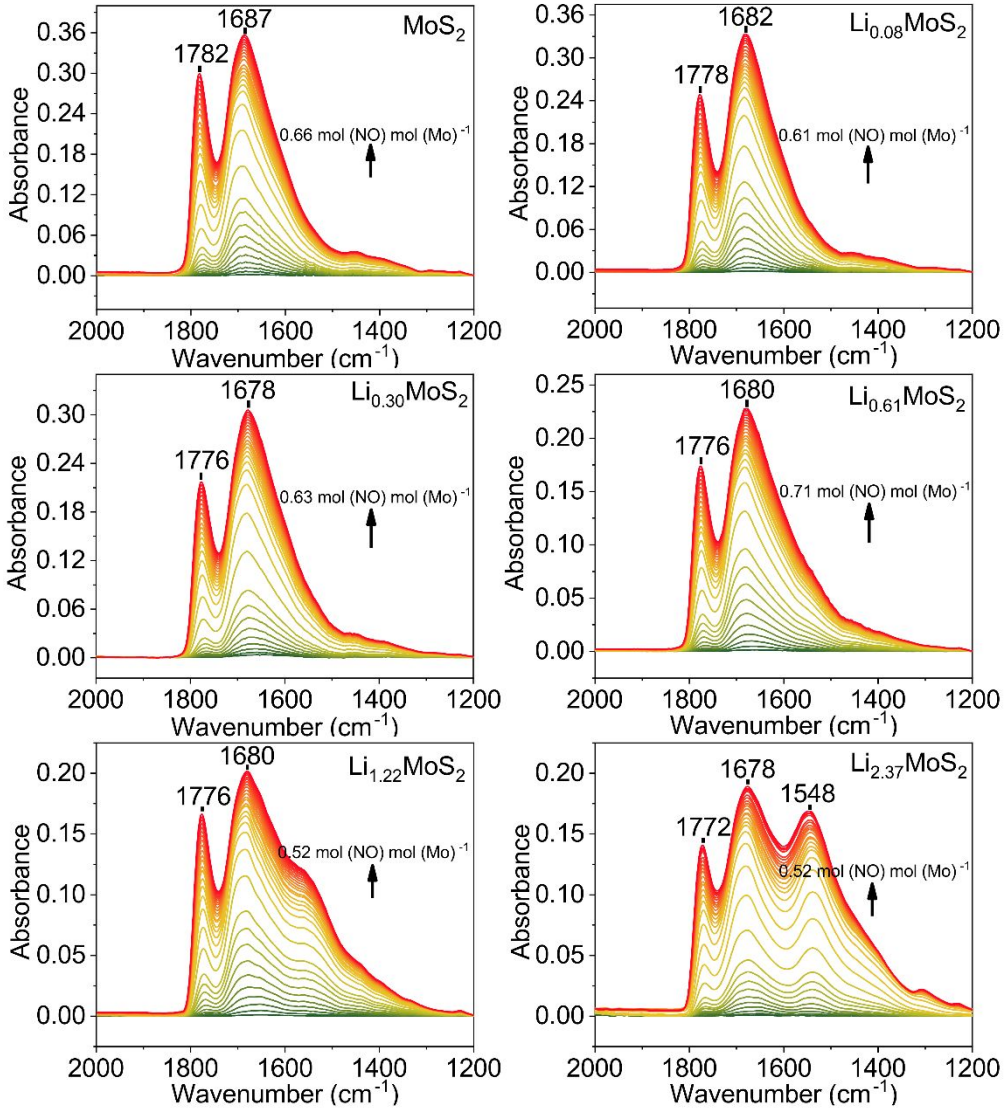

Figure S9. FTIR spectra of incremental doses of NO adsorbed on Li_xMoS_2/Al_2O_3 pellets up to an equilibrium coverage of NO molecules.

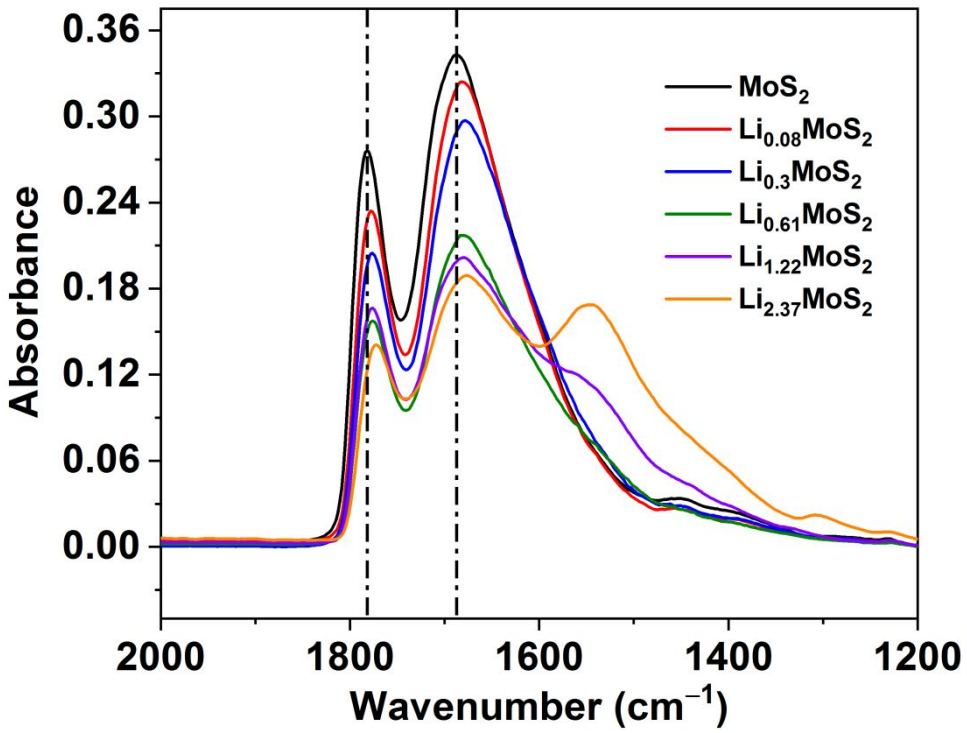

Figure S10. FTIR spectra of Li_xMoS_2/Al_2O_3 after dosing NO with a molecular ratio of 0.52 to Mo.

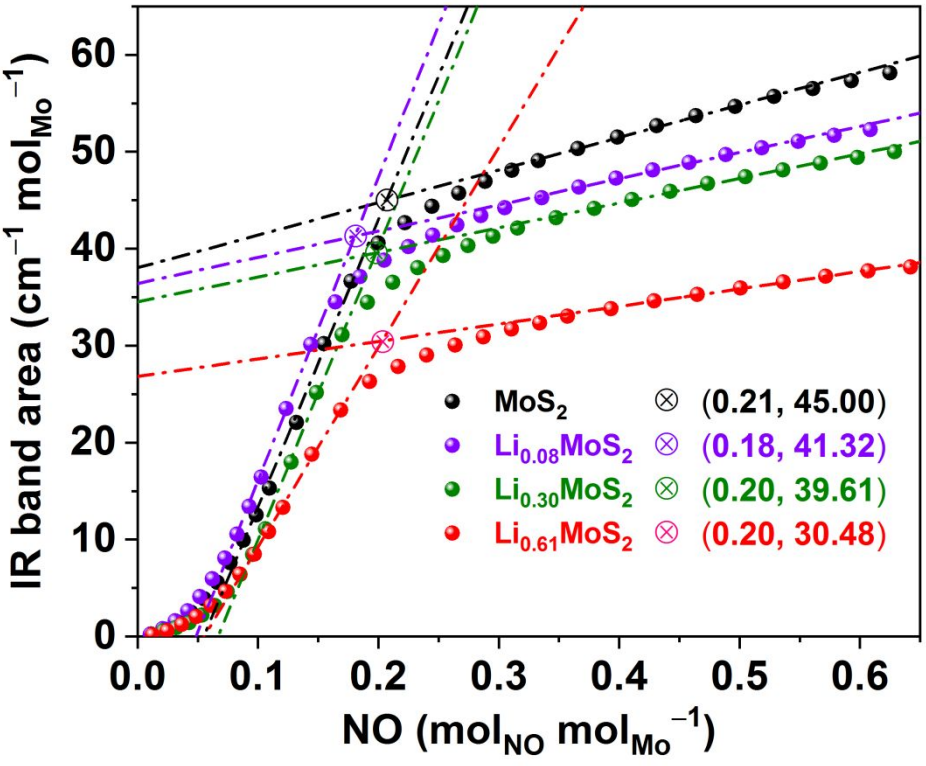

Figure S11. NO titration curve of Li_xMoS_2/Al_2O_3 with IR band area integrated between 1500 and 1810 cm^{-1}. The NO uptake was determined by the intersect between fitted linear lines of chemisorption and physisorption.

Even though the ^{7}Li NMR spectra provide valuable insights into the interaction between Li ions and MoS_2, information about the edge structure of MoS_2 in the presence of Li is still missing. However, such information can

be obtained indirectly via the adsorption of probe molecules monitored by infrared vibrational spectroscopy (IR).[1] Here, we have used NO as the probe molecule as it preferentially adsorbs on edge and corner sites of MoS_2, thereby yielding insight into the properties of those sites.[16, 17] Figure 2e and Figure S9 and 10 display the scheme of NO adsorption on Li_xMoS_2. A gradual red-shift of the IR bands at ~1782 cm^{-1} (coupled mononitrosyl or dinitrosyl, symmetric stretch, ν_s) and ~1687 cm^{-1} (coupled mononitrosyl or dinitrosyl, asymmetric stretch, ν_{as}) (Figure 2e, Figure S10) is observed upon introduction of Li ions, which can be ascribed to the fact that Li increases the electron density of Mo atoms which is then back-donated to NO 2π* orbitals. Importantly, quantitative NO adsorption may provide valuable information about the number of exposed edge sites (assigned as active sites). An objective comparison of the intrinsic properties of electrocatalyst activity requires knowledge of the electrochemically active surface area (ECSA), a parameter which often remains unknown. Here, the quantification of the number of edge sites makes it possible to derive more accurately structure-function correlations.[18-20] As shown in Figure S11, the NO titration curves of Mo display an NO uptake of ~0.2 mol_{NO} mol_{Mo}^{-1} for Li_xMoS_2.

Part VII: Bond structure in Li_xMoS_2

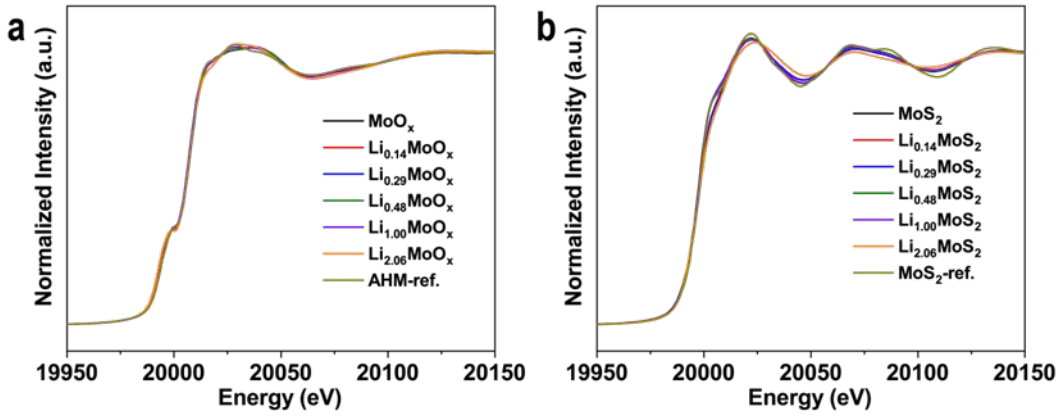

Figure S12. *Ex-situ* XANES spectra of Mo precursors (AHM) loaded on carbon support before (a) and after (b) sulfurization.

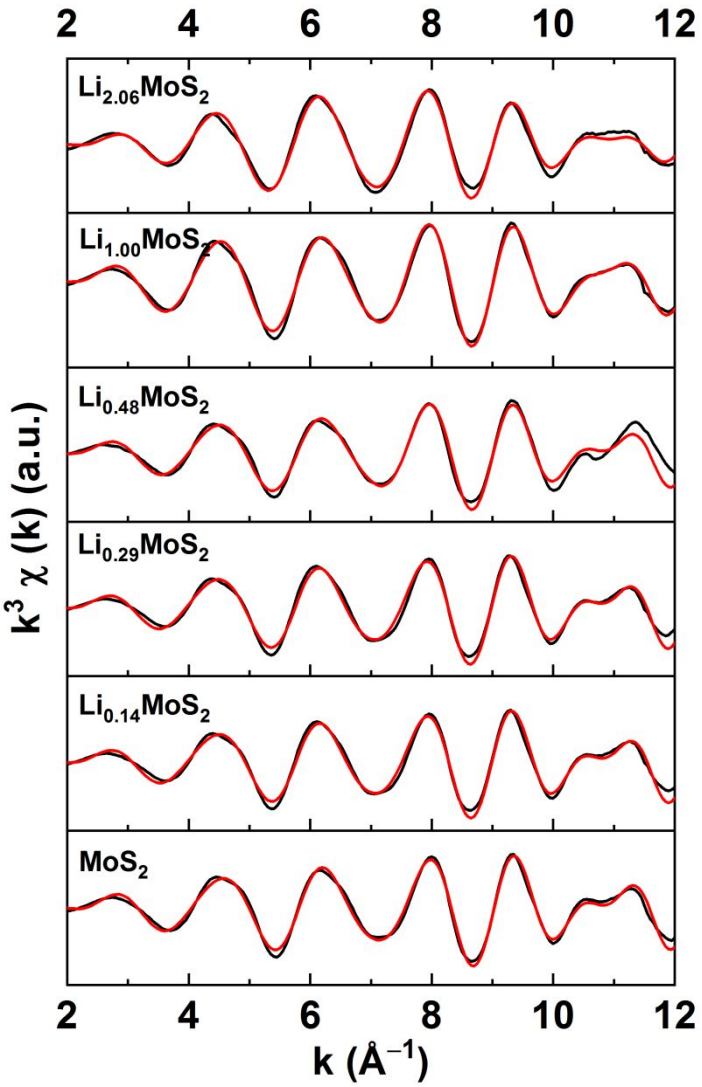

Figure S13. Mo-K edge EXAFS spectra plotted as χ (k) with k-weight of 3. Black curves represent experimental data and red curves show the fitted spectra.

Table S6: Average charge (Q) and variance with respect to the MoS_2 (ΔQ) for Mo and S atoms in a Li_xMoS_2 monolayer.

Species	**Mo**		**S**	
Charge	Q /e$^-$	$\lvert\Delta Q\rvert$ /e$^-$	Q /e$^-$	$\lvert\Delta Q\rvert$ /e$^-$
MoS_2	1.18		−0.59	
$Li_{0.13}MoS_2$	1.09	0.09	−0.61	0.02
$Li_{0.25}MoS_2$	1.10	0.08	−0.65	0.09
$Li_{0.31}MoS_2$	1.09	0.09	−0.70	0.11
$Li_{0.50}MoS_2$	1.04	0.14	−0.77	0.18
$Li_{1.00}MoS_2$	0.85	0.33	−0.90	0.31
$Li_{2.00}MoS_2$	0.64	0.54	−1.31	0.72

Table S7: DFT calculated Mo-S and Mo-Mo bond distances (Å) in a Li_xMoS_2 monolayer.

Sample name	**Mo-S**	**Mo-Mo**	**Short (Mo-Mo)**	**Li-S**	**Li-Mo**
MoS_2	2.421	3.192	---	---	---
$Li_{0.13}MoS_2$	2.419	3.145	2.947/3.638	2.213	2.871
$Li_{0.25}MoS_2$	2.418	3.146	2.921/3.802	2.328	3.002
$Li_{0.31}MoS_2$	2.402	3.146	2.885	2.332	2.975
$Li_{0.50}MoS_2$	2.316	3.228	2.902	2.258	3.051
$Li_{1.00}MoS_2$	2.429	3.122	2.740	2.299	2.799
$Li_{2.00}MoS_2$	2.460	3.294	2.802	2.331	2.950

Part VIII: Electrochemical characterization

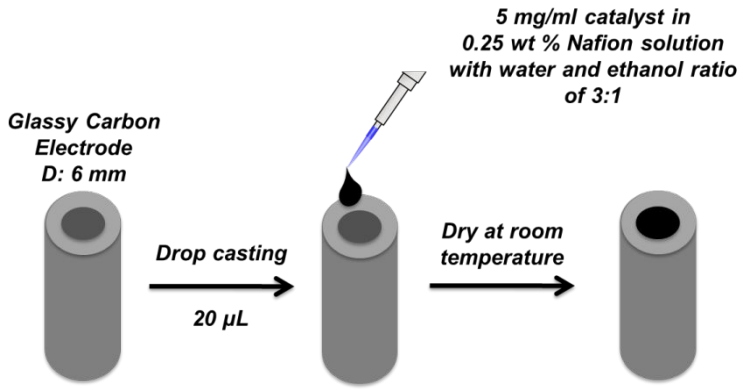

Figure S14. Scheme for the preparation of Li_xMoS_2/C electrodes for electrochemical characterizations.

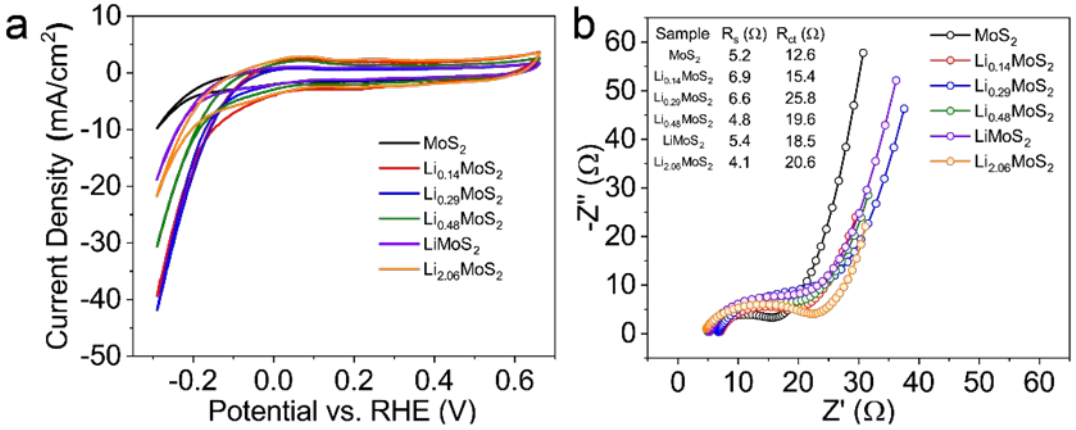

Figure S15. a) Cyclic voltammetry curves of Li_xMoS_2 in 0.1 M H_2SO_4 with rotating speed of 1600 rpm. Scan rate: 50 mV/s. b) Electrochemical impedance spectroscopy (EIS) collected at open circuit potential (V_{OCP}) in 0.1 M H_2SO_4 with an AC amplitude of 10 mV.

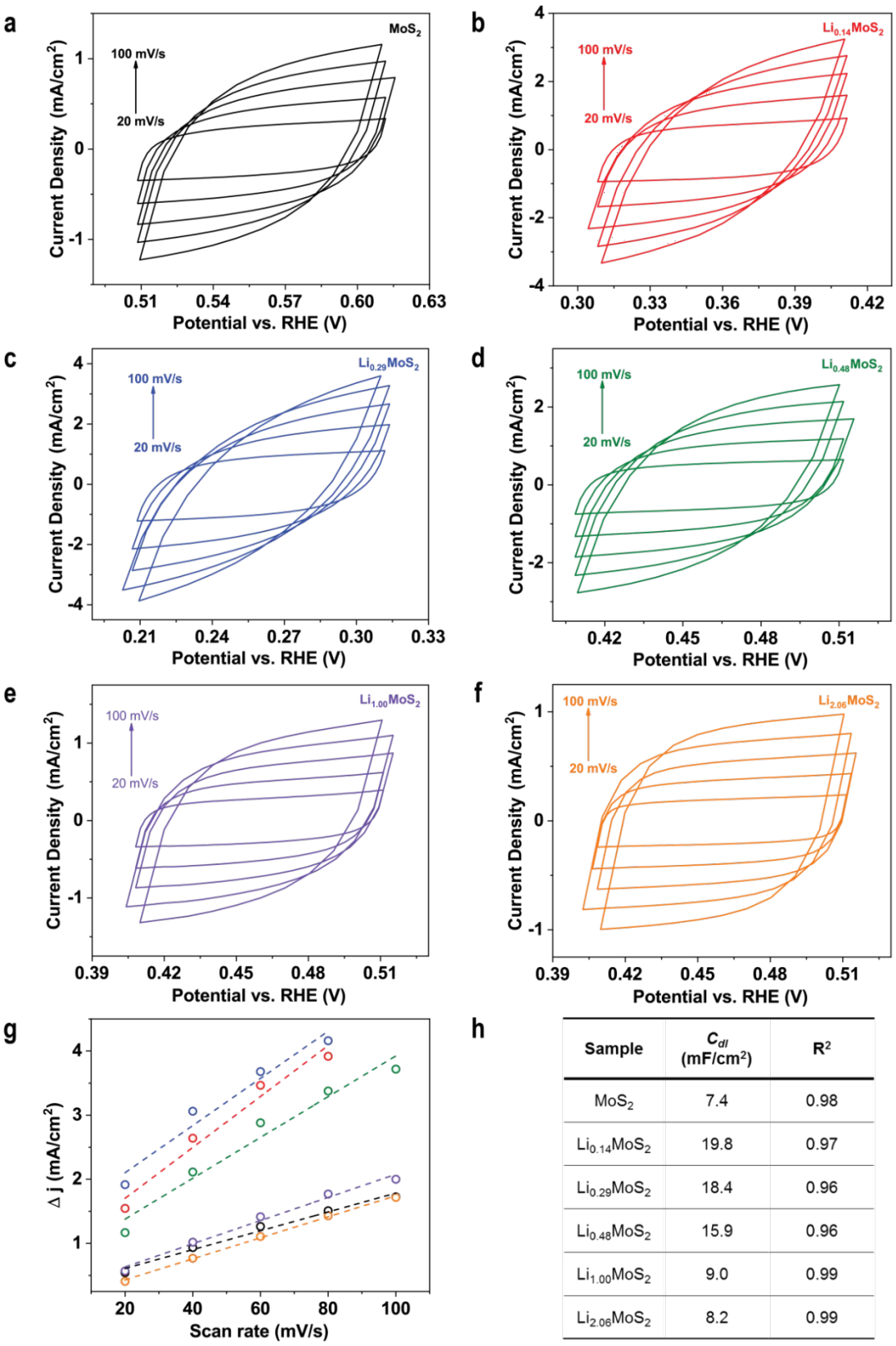

h

Sample	C_{dl} (mF/cm^2)	R^2
MoS_2	7.4	0.98
$Li_{0.14}MoS_2$	19.8	0.97
$Li_{0.29}MoS_2$	18.4	0.96
$Li_{0.48}MoS_2$	15.9	0.96
$Li_{1.00}MoS_2$	9.0	0.99
$Li_{2.06}MoS_2$	8.2	0.99

Figure S16. Electrochemical double layer capacitance (C_{dl}) measurements for Li_xMoS_2. a-f) Cyclic voltammetry (CV) measurements in the potential range of V_{OCP} (open circuit potential) ± 50 mV; g) fitting plots showing the extraction of corresponding C_{dl}; h) summary of C_{dl} obtained from fitting plots of (g). Color codes in g are the same used in panels a-f.

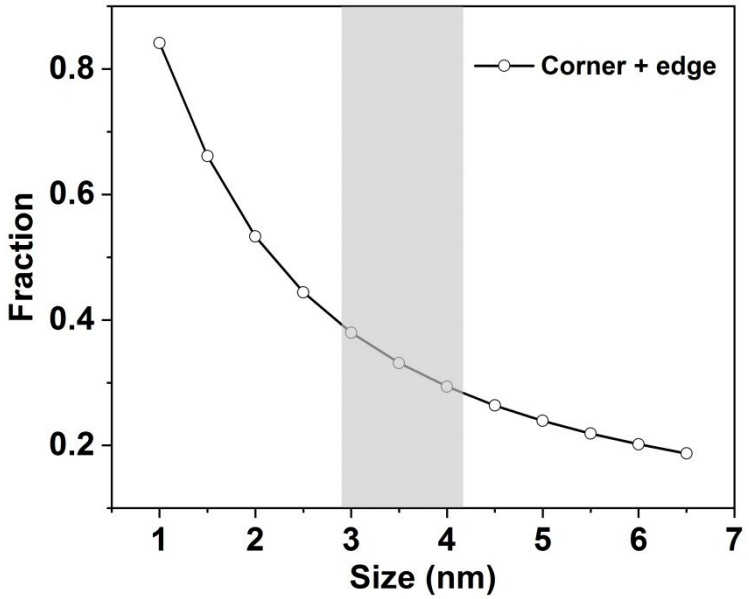

Figure S17. Calculated fraction of molybdenum atoms in hexagonal MoS_2 nanoparticles at corner and edge sites as a function of particle size.

Table S8. Calculated number of active sites (N_{active}) for Li_xMoS_2/C drop casted on glassy carbon electrodes based on NO titration (Figure S11)

Sample	N_{active} ***total***	N_{active} cm^{-1}
MoS_2	1.05×10^{16}	2.96×10^{15}
$Li_{0.14}MoS_2$	1.08×10^{16}	3.07×10^{15}
$Li_{0.29}MoS_2$	1.06×10^{16}	3.00×10^{15}
$Li_{0.48}MoS_2$	1.02×10^{16}	2.89×10^{15}
$Li_{1.00}MoS_2$	1.00×10^{16}	2.84×10^{15}
$Li_{2.06}MoS_2$	8.26×10^{15}	2.33×10^{15}

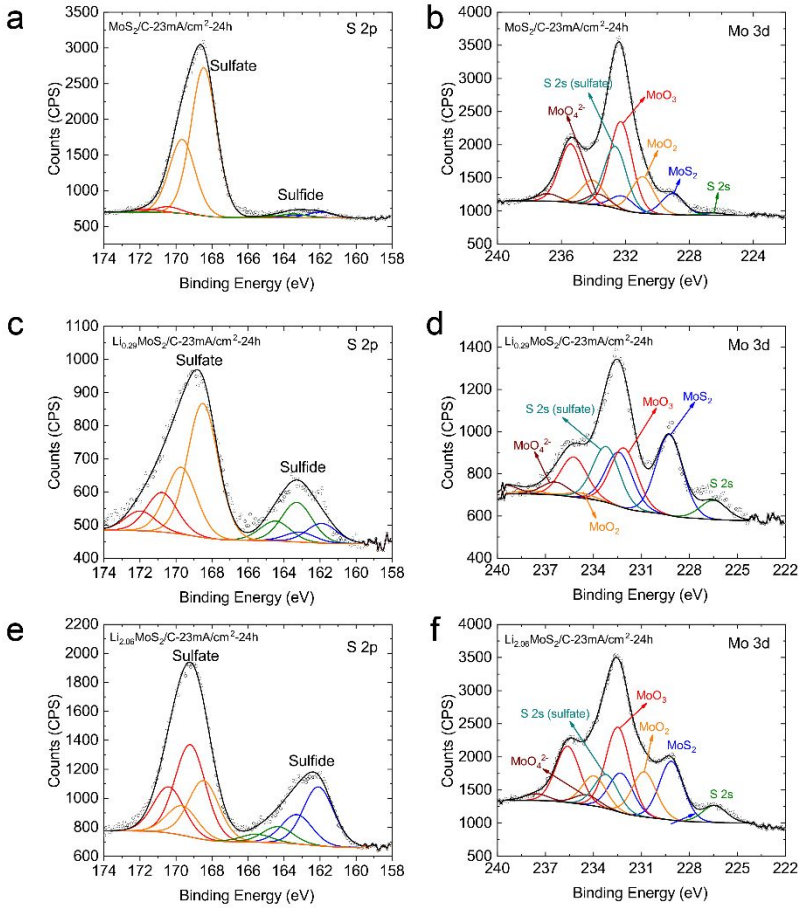

g

Sample	S 2p		Mo 3d			
	Sulfide (at. %)	Sulfate (at. %)	MoS_2 (at. %)	MoO_3 & MoO_2 (at. %)	MoO_4^{2-} (at. %)	S 2s (at. %)
MoS_2/C-23mA/cm²-24h	3.6	96.4	7.5	44.6	2.0	45.9
$Li_{0.29}MoS_2$ /C-23mA/ cm²-24h	25.5	74.5	26.8	21.5	2.2	49.5
$Li_{2.06}MoS_2$/ C-23mA/ cm2-24h	33.2	66.8	20.0	43.9	1.7	34.4

Figure S18. XP spectra of S 2p (a, c, e) and Mo 3d (b, d, f) for Li_xMoS_2 catalysts after HER stability test at 23 mA/cm² for 24 h. g, Summary of atomic ratios of different components based on XPS analysis of S 2p and Mo 3d.

According to the Pourbaix diagrams reported for the Mo-H_2O-S system in the literature[21,22], the Li_xMoS_2 materials have been operated in the stability window of MoS_2 during long term HER stability testing (pH ~0.7, −0.5 V < E_{RHE} < −0.2 V). We therefore surmise that the observed oxidation (XPS) (Figure S18) is due to exposure of the samples to moist air after catalytic testing.

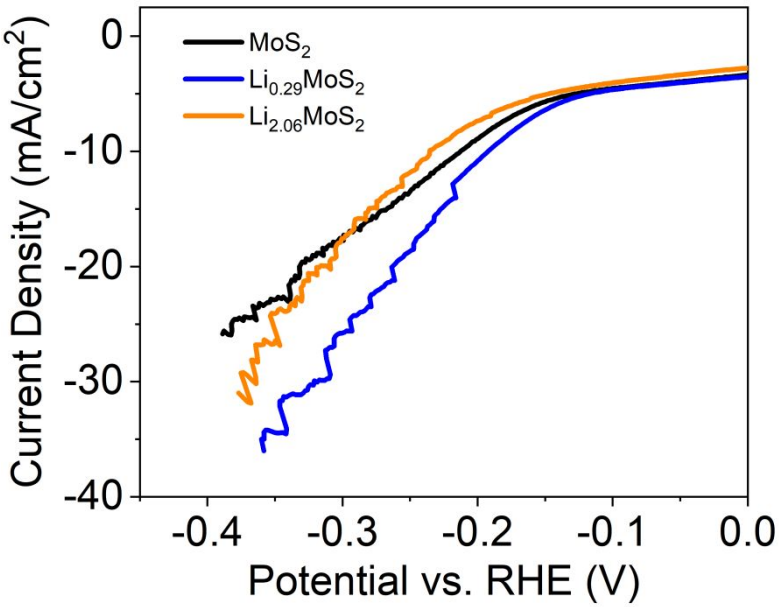

Figure S19. Linear sweep voltammetry (LSV) curves (corrected by uncompensated resistance) of Li_xMoS_2 catalysts on glassy carbon electrode (GCE) after washing with MilliQ water.

Part IX: Raman spectroscopy

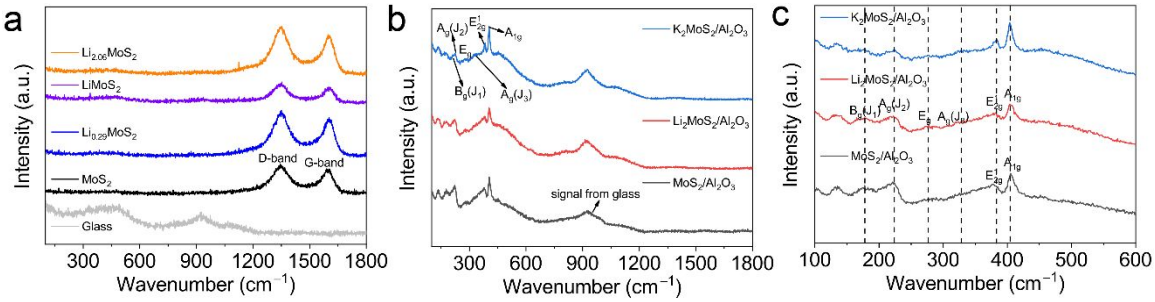

Figure S20. Raman spectra of C-supported Li_xMoS_2 catalysts (a) with increasing lithium content and A_2MoS_2 (A=Li, K) on γ-Al_2O_3 (b, c). Samples were sealed in a glovebox on a glass slide with Kapton tape and a glass coverslip to protect samples from air exposure during Raman measurements.

Part IIX: Hydrogen adsorption on Li_xMoS_2

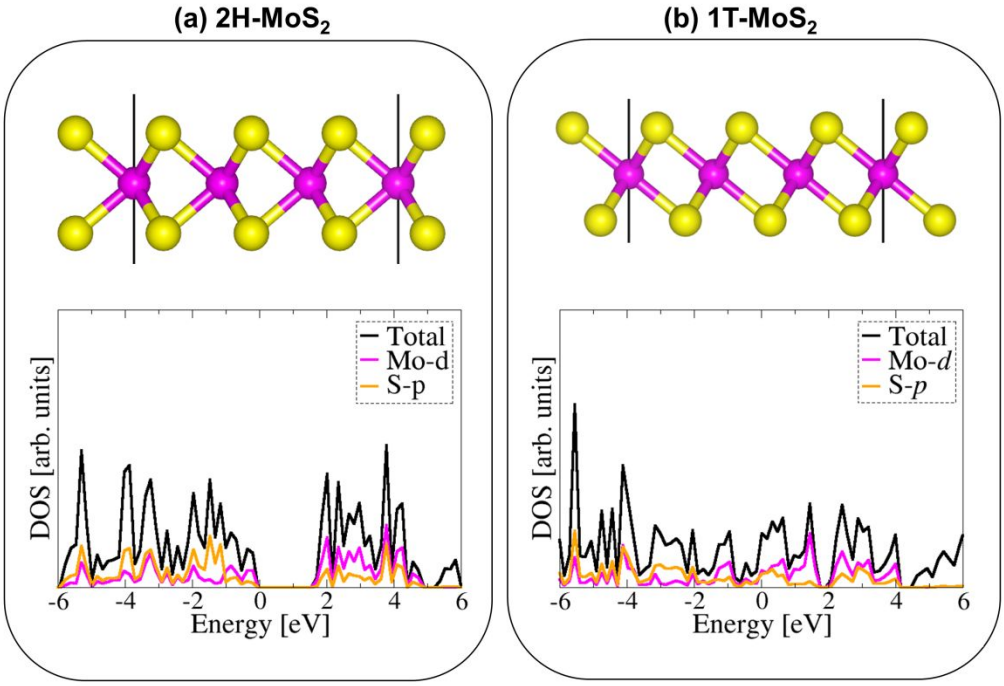

Figure S21. Structures and PDOS (partial density of state) of 2H (a) and 1T (b) MoS_2 monolayers. The Fermi level is located at 0 eV.

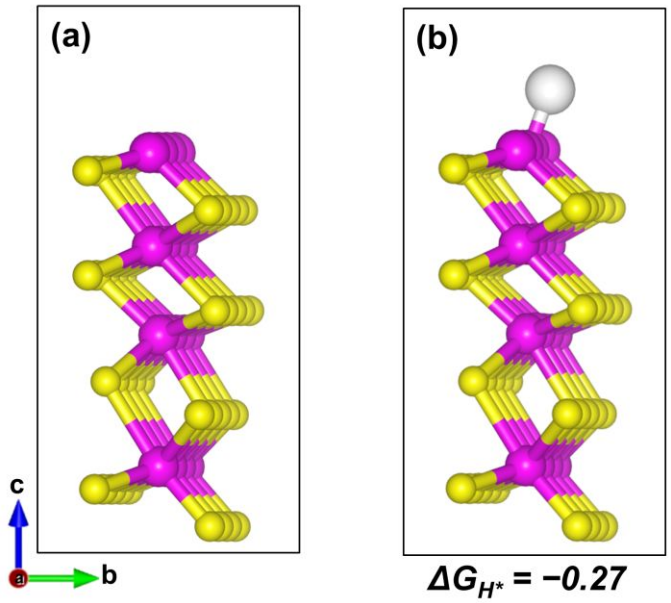

Figure S22. Structure of pristine Mo-edge of 1T-MoS_2 monolayer without (a) and with (b) hydrogen adsorption. Vacuum size in the *c*-direction perpendicular to the Mo-edge is 20 Å.

Table S9. Calculated vibrational frequencies of H adsorbed on the Mo-edge of Li_xMoS_2 monolayer with different Li concentrations.

	ν (H adsorbed) cm^{-1}		
MoS_2	1815.039	405.1186	344.175
$Li_{0.13}MoS_2$	1714.376	913.126	572.289
$Li_{0.25}MoS_2$	1551.974	848.863	230.782
$Li_{0.31}MoS_2$	1676.075	998.345	231.534
$Li_{0.50}MoS_2$	1676.900	895.399	418.019
$Li_{1.00}MoS_2$	1478.690	826.382	449.450
$Li_{2.00}MoS_2$	1484.766	936.590	459.449

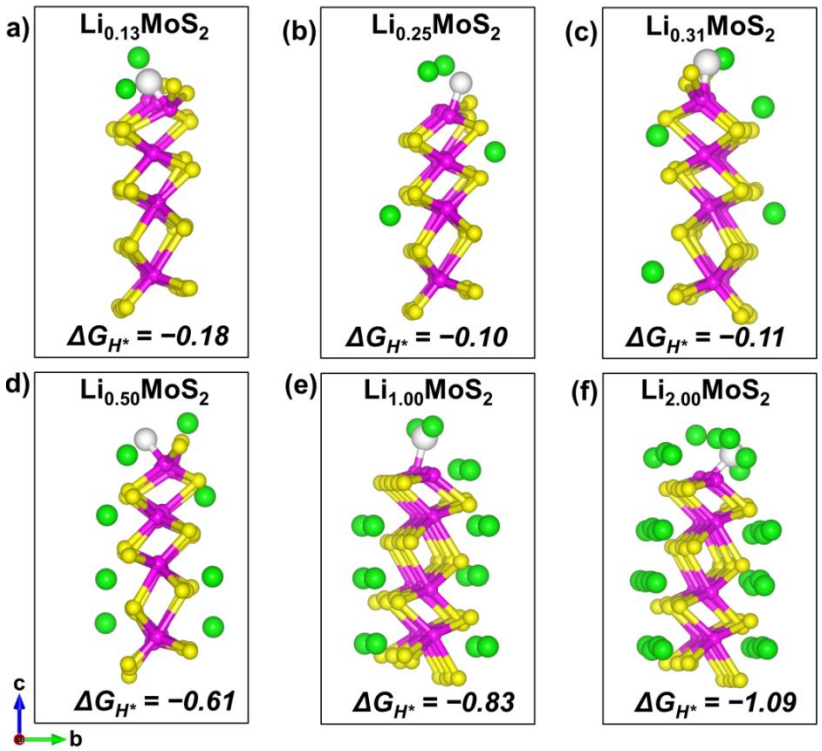

Figure S23. Calculated Gibbs free energy (eV) for hydrogen adsorption on Mo-edge of Li_xMoS_2 monolayer with different Li concentrations. a, $Li_{0.13}MoS_2$; b, $Li_{0.25}MoS_2$; c, $Li_{0.31}MoS_2$; d, $Li_{0.50}MoS_2$; e, $Li_{1.00}MoS_2$; f, $Li_{2.00}MoS_2$. Vacuum size in the *c* direction perpendicular to the Mo-edge is 20 Å.

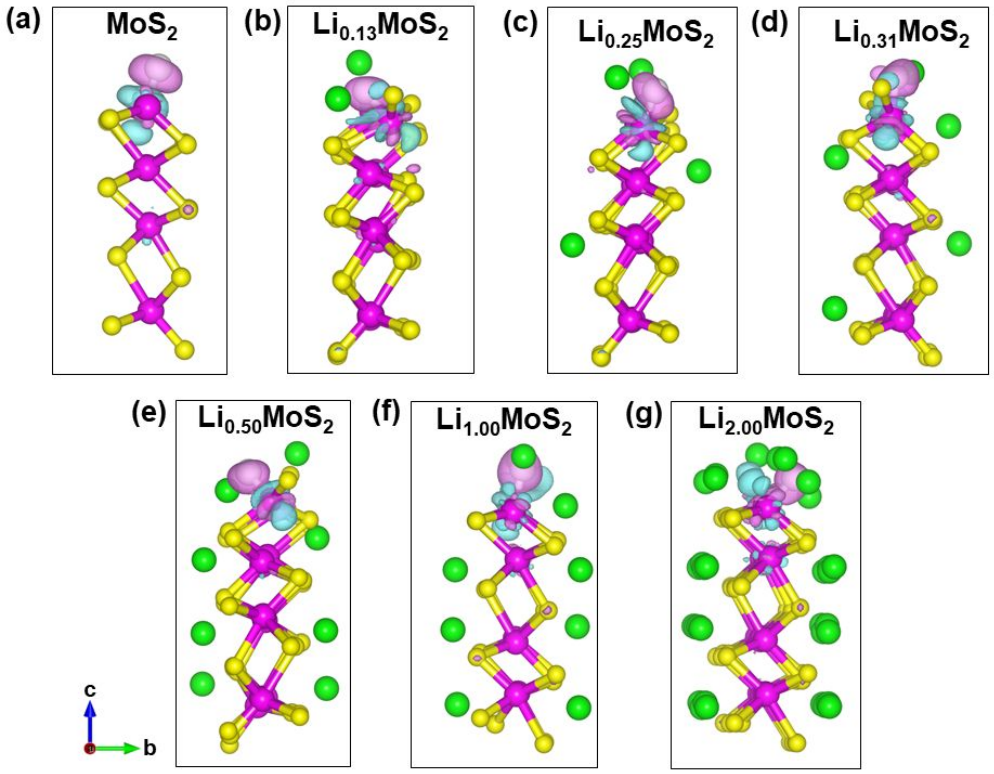

Figure S24. Electron density difference isosurface contours of H adsorption Mo-edge of Li_xMoS_2 monolayer with different Li concentrations, where the pink and cyan contours indicate electron density increase and decrease by 0.02 e^{-} $Å^{-3}$, respectively. a, MoS_2; b, $Li_{0.13}MoS_2$; c, $Li_{0.25}MoS_2$; d, $Li_{0.31}MoS_2$; e, $Li_{0.50}MoS_2$; f, $Li_{1.00}MoS_2$; g, $Li_{2.00}MoS_2$.

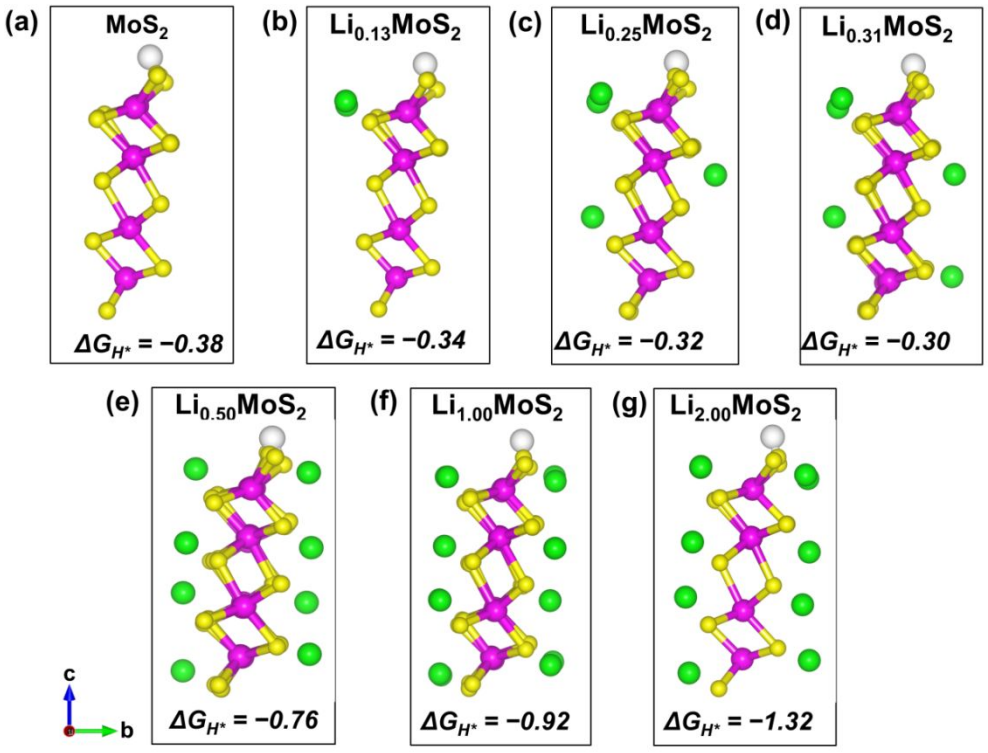

Figure S25. Calculated Gibbs free energy (eV) for hydrogen adsorption on S-edge of Li_xMoS_2 monolayer with different Li concentrations. Vacuum size in the c direction perpendicular to the Mo-edge is of 20 Å. a, MoS_2; b, $Li_{0.13}MoS_2$; c, $Li_{0.25}MoS_2$; d, $Li_{0.31}MoS_2$; e, $Li_{0.50}MoS_2$; f, $Li_{1.00}MoS_2$; g, $Li_{2.00}MoS_2$.

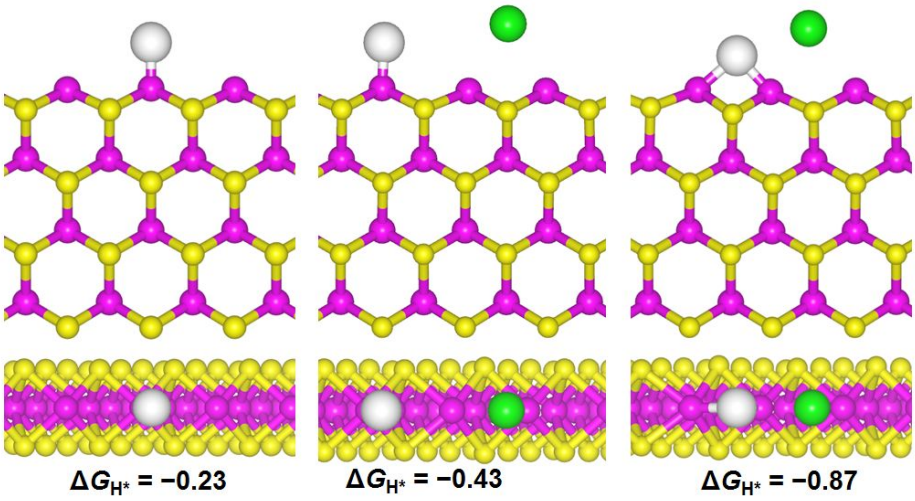

Figure S26. Calculated Gibbs free energies (eV) for hydrogen adsorption on Mo-edges of 2H-MoS_2 monolayer with and without Li adsorption. Vacuum size in the *c* direction perpendicular to the Mo-edge is 20 Å.

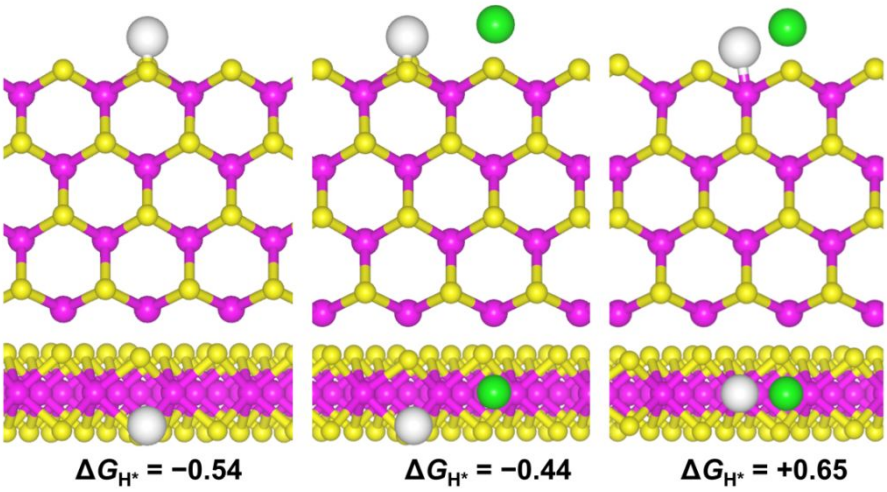

Figure S27. Calculated Gibbs free energy (eV) for hydrogen adsorption on S-edges of 2H-MoS_2 monolayer with and without Li adsorption. Vacuum size in the *c* direction perpendicular to the S-edge is 20 Å.

References

1. van Haandel, L.; Hensen, E. J. M.; Weber, Th. FT-IR Study of NO Adsorption on MoS_2/Al_2O_3 Hydrodesulfurization Catalysts: Effect of Catalyst Preparation. *Catalysis Today* **2017**, *292*, 67-73.
2. Kresse, G.; Furthmüller, J. Efficiency of Ab-initio Total Energy Calculations for Metals and Semiconductors Using a Plane-wave Basis set. *J. Comput. Mat. Sci.* **1996**, *6*, 15−50.
3. Kresse, G.; Hafner, J. Ab Initio Molecular Dynamics for Liquid Metals. *J. Phys. Rev. B.* **1993**, *47*, 558-561.
4. Blöchl, P. E. Projector Augmented-wave Method. *Phys. Rev. B.* **1994**, *50*, 17953-17979.
5. Perdew, J. P.; Burke, K. Ernzerhof, M. Generalized Gradient Approximation Made Simple. *Phys. Rev. Lett.* **1996**, *77*, 3865−3868.
6. Monkhorst, H. J.; Pack, J. D. Special Points for Brillouin-zone Integrations. *Phys. Rev. B.* **1976**, *13*, 5188−5192.

7. Grimme, S.; Antony, J.; Ehrlich, S.; Krieg, S. A Consistent and Accurate Ab Initio Parametrization of Density Functional Dispersion Correction (DFT-D) for the 94 Elements H-Pu. *J. Chem. Phys*. **2010**, *132*, 154104.
8. Tang, Q.; Jiang, D.-e. Stabilization and Band-Gap Tuning of the 1T-MoS_2 Monolayer by Covalent Functionalization. *Chem. Mater*. **2015**, *27*, 3743−3748.
9. Henkelman, G.; Arnaldsson, A.; Jónsson, H. A Fast and Robust Algorithm for Bader Decomposition of Charge Density. *Comput. Mater. Sci*. **2006**, *36*, 354−360.
10. Bagus, P. S.; Illas, F.; Pacchioni, G.; Parmigiani, F. Mechanisms Responsible for Chemical Shifts of Core-level Binding Energies and Their Relationship to Chemical Bonding. *J. Electron Spectros. Relat. Phenomena*, **1999**, *100*, 215-236.
11. Bellafont, N. P.; Viñes, F.; Hieringer, W.; Illas, F. Predicting Core Level Binding Energies Shifts: Suitability of the Projector Augmented Wave Approach as Implemented in VASP. *J. Comput. Chem*. **2017**, *38*, 518–522.
12. Bellafont, N. P.; Viñes, F.; Illas, F. Performance of the TPSS Functional on Predicting Core Level Binding Energies of Main Group Elements Containing Molecules: A Good Choice for Molecules Adsorbed on Metal Surfaces *J. Chem. Theory Comput.* **2016**, *12*, 324-331.
13. Bellafont, N. P.; Saiz, G. A.; Viñes, F.; Illas, F. Performance of Minnesota Functionals on Predicting Core-level Binding Energies of Molecules Containing Main-group Elements. *Theor. Chem. Acc.* **2016**, *135*, 35.
14. Jiao, Y.; Zheng, Y.; Jaroniec, M.; Qiao, S. Z. Design of Electrocatalysts for Oxygen- and Hydrogen-involving Energy Conversion Reactions. *Chem. Soc. Rev.* **2015**, *44*, 2060–2086.
15. Greeley, J.; Jaramillo, T. F.; Bonde, J.; Chorkendorff, I.; Nørskov, J. K. Computational High-throughput Screening of Electrocatalytic Materials for Hydrogen Evolution. *Nat. Mater.* **2006**, *5*, 909-913.
16. Nørskov, J. K.; Bligaard, T.; Logadottir, A.; Kitchin, J. R.; Chen, J. G.; Pandelov, S.; Stimming, U. Trends in the Exchange Current for Hydrogen Evolution. *J. Electrochem. Soc.* **2005**, *152*, J23-J26.
17. Topsøe, N. Y.; Topsøe, H. Characterization of the Structures and Active Sites in Sulfided Co-Mo/Al_2O_3 and Ni-Mo/Al_2O_3 Catalysts by NO Chemisorption. *J. Catal.* **1983**, *84*, 386-401.
18. Yoon, Y.; Yan, B.; Surendranath, Y. Suppressing Ion Transfer Enables Versatile Measurements of Electrochemical Surface Area for Intrinsic Activity Comparisons. *J. Am. Chem. Soc.* **2018**, *140*, 2397-2400.
19. McCrory, C. C.; Jung, S.; Ferrer, I. M.; Chatman, S. M.; Peters, J. C.; Jaramillo, T. F. Benchmarking Hydrogen Evolving Reaction and Oxygen Evolving Reaction Electrocatalysts for Solar Water Splitting Devices. *J. Am. Chem. Soc.* **2015**, *137*, 4347-4357.
20. Hinnemann, B.; Moses, P. G.; Bonde, J.; Jørgensen, K. P.; Nielsen, J. H.; Horch, S.; Chorkendorff, I.; Nørskov, J. K. Biomimetic Hydrogen Evolution: MoS_2 Nanoparticles as Catalyst for Hydrogen Evolution. *J. Am. Chem. Soc.* **2005**, *127*, 5308-5309.
21. Huang, Y.; Nielsen R. J.; Goddard III, W. A.; Soriaga, M. P. The Reaction Mechanism with Free Energy Barriers for Electrochemical Dihydrogen Evolution on MoS_2. *J. Am. Chem. Soc.* **2015**, *137*, 6692-6698.
22. Davoodi, A.; Pakshir, M.; Babaiee, M.; Ebrahimi, G.R. A Comparative H_2S Corrosion Study of 304L and 316L Stainless Steels in Acidic Media. *Corrosion Sci.* **2011**, *53*, 399-408.